Classification and Assessment of Propeller Faults in Electric Unmanned Aerial Vehicle Drive Trains

Immo Schmidt[1]

[1] *Institute of Flight Systems and Automatic Control, Technical University of Darmstadt, Otto-Berndt-Str. 2, 64287 Darmstadt, Germany*
schmidt@fsr.tu-darmstadt.de

ABSTRACT

Propellers are critical to the safe operation of multicopter unmanned aerial vehicles (UAVs), as faults can decrease the efficiency of the propulsion system and affect flight performance. Depending on the type and extent of the fault, the effects can range from a slight reduction in performance to a significant loss of thrust that could compromise safety. Because of the limited amount of sensor data available on board a UAV, propeller damage cannot be measured directly. Therefore, a data-based prediction using available sensors is required. This paper focuses on establishing and predicting a health index for damaged propellers. A test bench is used to investigate the effects of two different types of damage: broken propeller tips and notches at the leading edge. Each type of damage is examined at three levels of severity. Based on sensor data collected from the test bench, a health index is defined to characterize the remaining performance of the damaged propellers. A two-stage approach for the data-based health prediction is implemented by first classifying the type of the propeller faults, and then employing a random forest regressor to estimate the remaining health.

1. INTRODUCTION

The use of unmanned aerial vehicles (UAVs) in both civil and military applications is rising. Among the many fields of application are agriculture, inspection, and delivery. During their operation, there is a need for high safety, as crashes may lead to fatal consequences, especially when flying over populated areas. Multicopters are a popular type of UAV because they can take off and land vertically. They are driven by multiple electric drive trains that deliver the necessary thrust to generate lift. The drive trains typically consist of the components battery, electronic speed converter (ESC), brushless direct current (BLDC) motor and propeller.

Since a fault in any of the components can reduce the amount of generated thrust, they are crucial to the safety of unmanned aerial vehicles. During the operation of UAVs, mechanical damage to the propellers occurs frequently. Propellers can be damaged by collisions with small particles or during landings, which can result in notches on the propeller surface or broken blades. Because of that, propeller faults are of high criticality (Wolfram & Vogel, 2017). In a survey among drone operators, (Osborne et al., 2019) also identified propeller blades as one of the mechanical components with the highest probability of failure. Consequently, the present study concentrates on the detection and analysis of propeller faults.

The impact of various propeller faults on UAV flight performance has been the subject of several scientific studies. (Wolfram, Vogel, & Stauder, 2018) investigated the influence of notch faults and surface abrasion, proposing a condition monitoring concept that examines the input and output power of drive train components. (Brulin, Khenfri, & Rizoug, 2024) generated both simulated and experimental data for propellers with broken blades and characterized the difference in thrust and torque caused by these faults. In their research on lift estimation for multirotor systems, (Baldini et al., 2024) complemented an analysis of the impact of propeller faults by examining the effect of varying battery discharge and compared the effects of both propeller and battery components on the generation of thrust.

To ensure the safe operation of UAVs, faults in any component of the drive train must be reliably detected. In addition to traditional model-based approaches, data-driven approaches have gained popularity in recent years within the domain of fault detection (Puchalski & Giernacki, 2022). An approach for detecting broken propellers based on acceleration and current data was presented by (Pourpanah, Zhang, Ma, & Hao, 2018). (Benini, Ferracuti, Monteriu, & Radensleben, 2019) utilized time- and frequency domain analysis of high-rate acceleration data from the inertial measurement unit to diagnose propeller damage.

The consequences of a fault depend heavily on its size and

severity. Therefore, an estimation of the extent of the damage is necessary for predicting the consequences associated with the detected faults. Diagnosing the type and severity of a fault provides important information about its impact on UAV flight performance. In this research direction, an approach to diagnosis that extends beyond fault detection was implemented by (Bondyra, Gasior, Gardecki, & Kasinski, 2017). They developed a three-stage algorithm that detects the occurrence of propeller faults, distinguishes between two different types of faults, and estimates the severity of the fault by differentiating between the two classes of light and severe faults. (Pose, Giribet, Torre, & Marzik, 2023) presented a regression approach that uses a neural network trained on spectral bands of accelerometer and gyroscope sensor data to estimate the size of damage for cut propeller tips.

Within this paper, the goal is to establish a generalized health index that can be applied to different types of faults. Based on the defined health index, a two-stage approach is implemented for the purpose of classifying propeller fault types and assessing the remaining propeller health for each fault type. This quantification of damage severity can be used to estimate the remaining drive train performance and support further mission planning.

The paper is structured as follows: Section 2 provides an overview of the test rig and the experimental setup used to quantify the effect of different types of damage on drive train performance. The measured data is analyzed in Section 3 and a health index is defined. In Section 4, the modeling approach for classification and health estimation is described. The results of the generated models are shown in Section 5, followed by a conclusion.

2. EXPERIMENTAL SETUP

To quantify the effects of damage on the performance of the propulsion system, a test bench has been developed. The test bench offers the advantage that even severe damage can be tested in a safe environment without risking a UAV crash. Additionally, it is easy to measure the thrust and torque of the powertrain under static test bench conditions, whereas this information is generally unavailable from UAV flight data.

2.1. Test Bench Design

Figure 1 shows the test bench setup. It includes the main components of a UAV drive train. A battery serves as the electric power supply. The ESC converts the battery's direct current into three-phase alternating current, which the BLDC motor then transforms into mechanical rotation. The motor drives a propeller, generating the thrust force. The test bench is controlled via pulse width modulation (PWM) inputs to the ESC. Different speeds are achieved by adjusting the PWM duty cycle.

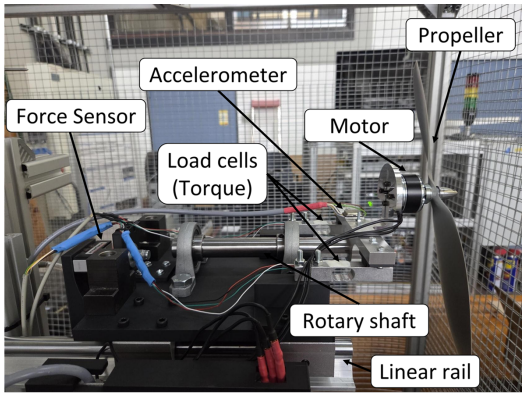

Figure 1. Setup of the test bench. Battery and ESC components are outside of the captured image.

The test bench is equipped with sensors that measure the mechanical and electrical performance of the drive train. Measured quantities include:

- thrust,
- torque,
- three-axial vibration,
- rotational speed,
- battery supply voltage, and
- battery supply current.

The motor and propeller are mounted on a connecting plate that is fixed to a rotary shaft. Two load cells attached to the outside of the connecting plate measure the torque generated by the motor. The shaft, along with the components mounted on it, is in turn positioned on a linear rail. During operation, the thrust generated by the propeller is transmitted to a force sensor via the linear motion and is then measured. Additionally, an accelerometer measures the resulting vibrations in three axes. The propeller's rotational speed is determined by an optical sensor. Current and voltage are measured between the battery and the ESC.

2.2. Experimental Runs

All test bench runs analyzed in this paper were carried out using the same electric drive train. The motor used is a T-Motor Navigator Type MN3110 KV700, which drives an APC Slowfly 12x3.8 inch propeller. A four-cell lithium polymer battery supplies the electric power.

To investigate the influence of various types of damage, the propellers are damaged in two different ways. On the one hand, the influence of broken propeller tips is investigated as an example of faults that can severely impact flight performance depending on the damage size. To realize this type of damage, part of the propeller tip is cut off either on one of the two blades or on both blades. On the other hand, damage in the form of small notches is created on the leading edges

Table 1. Definition of the types of damage introduced to the propeller and their associated severity grades.

Type of damage	Grade A	Grade B	Grade C
Broken tip	5 mm	10 mm	20 mm
Leading edge notches	1 notch	2 notches	3 notches

Figure 2. Depiction of damage types: no fault, one broken tip, two broken tips, notches at the leading edge of both blades (from left to right).

of the propellers. This simulates minor damage that has less of an impact on thrust generation, but is frequently observed during UAV operation. For example, it can result from hard landings. The notches have a uniform size of 6 mm in width and 3 mm in depth, and are also either applied to only one of the blades or to both. Figure 2 shows examples of the different types of damage. All damage types are introduced in three different gradations. For the cut-off propeller tips, propellers with blade lengths reduced by 5 mm, 10 mm, and 20 mm are used. For the notches on the leading edge of the propeller, the severity grades differ in that the number of notches of the same size increases from one notch to three notches. A summary of the introduced damages is shown in Table 1.

A uniform duty cycle step profile with five distinct duty cycles is run for each propeller. The five duty cycle inputs cover the entire operating range of the drive train. To increase variance in the dataset, multiple test runs are carried out with the same propeller at different battery states of charge. Due to the varying state of charge, the same duty cycle input may result in different propeller speeds.

3. EFFECT OF DAMAGES ON DRIVE TRAIN PERFORMANCE

The primary function of the drive train is to generate thrust, which mainly depends on the propeller's rotational speed. Once the measured values of thrust and propeller speed are

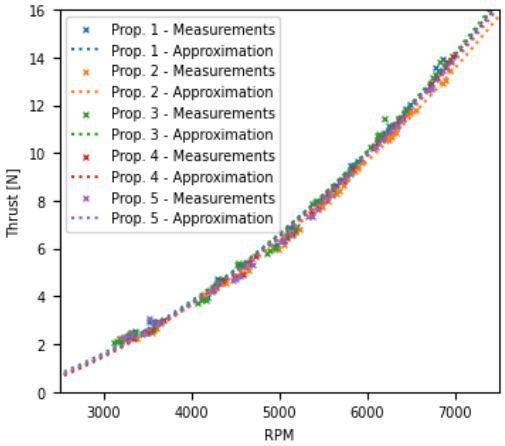

Figure 3. Thrust curves of undamaged propellers.

known, the thrust coefficient c_T is determined as:

$$c_T = \frac{T}{\rho D^4 N^2} \tag{1}$$

with N being the propeller speed, ρ the air density, D the diameter of the propeller and T the measured thrust. The thrust coefficient varies for each propeller. In general, it is not constant, but rather depends on several factors, such as the incoming flow velocity. However, under static conditions on the test rig and within a limited range of propeller speeds, it is assumed to remain nearly constant. This is an ideal assumption that does not exactly hold true in reality, partly due to disturbances in the airflow caused by the test bench setup.

The thrust coefficient decreases when damage is introduced to the propeller. In that case, the propeller delivers less thrust at the same speed. To quantify the effect of different types of damage, a health index (HI) is proposed, which defines propeller health as the ratio of the thrust coefficient of the damaged propeller to that of an undamaged propeller.

$$\mathrm{HI} = \frac{c_{T,damaged}}{c_{T,undamaged}} \tag{2}$$

To characterize the behavior of undamaged propellers, the thrust of five identical propellers was measured and compared. The resulting graph in Figure 3 shows the dependency of thrust on the rotational speed of the propellers. All measurement points represent the mean thrust value over two seconds with a constant duty cycle input. For each propeller, the step profile with five different duty cycles was run nine times with a varying battery state of charge. Consequently, there are 45 measurement points per propeller.

The thrust coefficient is calculated using a quadratic regression approach that maps propeller speed to measured thrust. To minimize approximation error, the thrust curve is mod-

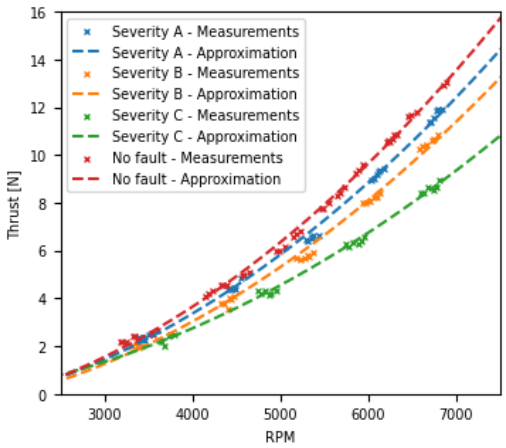

Figure 4. Thrust Curve of propellers with broken tip damage at both blades.

eled while allowing for a zero offset. Therefore, the estimated thrust coefficients are only valid within the considered speed range of 3,000 to 7,000 revolutions per minute (RPM).

$$T = T_0 + c_T \rho D^4 N^2 \tag{3}$$

This approach generates the approximated thrust curves of each propeller displayed in Figure 3. The root mean squared error of this approximation is at 0.2 newtons. While this shows that the assumption of a constant thrust coefficient is not exactly met, it provides adequate estimations within the propeller's normal operating range.

The five investigated propellers show similar behavior, with only minor variations in thrust generation. In summary, the observed thrust coefficients of the undamaged propellers are quantified by a median value of $c_{T,undamaged} = 0.1074$ and a maximum deviation of 3.2% from that median value.

Propeller blade damage is expected to reduce the thrust generated by the drive train. Figure 4 shows the thrust curves of a propeller with broken tip damage on both blades, which confirms this expectation. The measurements were taken with the same propeller, while gradually increasing damage from a healthy state to severity grade C. Two effects of broken tips are visible. First, thrust is significantly reduced, and the approximate thrust coefficients are distinctly lower than those of undamaged propellers. Second, damaged propellers reach higher rotational speeds at the same duty cycle input due to the lower air resistance of propellers with a reduced diameter.

A similar analysis was conducted for all types of damage included in this paper. Table 2 shows the resulting measured health indices. It has to be noted that the health index analysis was performed using only one propeller for each type of damage. Therefore, the analysis does not include information on statistical variation if similar damage were applied to different propellers. At a damage severity level of grade C, a propeller with two broken tips generates less than 70% of the thrust of the undamaged propeller at the same rotational speed. The other types of damage have a smaller impact on thrust generation. This is explained by the relatively little material that is removed to create these types of damage. In particular, the effect of small notches at the leading edge is minimal. While a steady decrease in thrust coefficient is observed with increasing damage severity, an additional notch leads only to a reduction in thrust coefficient of around $1-2\%$. This reduction falls within the statistical variation of undamaged propellers. In the case of a single notch on both blades, the health index is even measured to be slightly increased. The measured health indices are only below the lowest observed health index of an undamaged propeller at severity grade C.

4. MODELING APPROACH

For UAV applications, not all sensor data from the test bench is available. Generally, there is no method for measuring the thrust and torque generated by UAV drive trains during flight. Instead, thrust and torque can only be estimated based on the propellers' rotational speed and the data sheets from the propeller manufacturer. However, this method only works for undamaged propellers, since no appropriate data sheets are available for damaged propellers. Therefore, the input data for the fault detection algorithm is limited to measurements of supply voltage, electric current, rotational speed, and vibration.

Data collected on the test bench is used to develop methods for fault classification and health assessment. The dataset of five right-handed propellers presented in Section 3 was supplemented with a dataset of five additional left-handed propellers of the same design. Thus, a total of ten propellers were used for data recording. Out of five identical propellers, one each was damaged in accordance with the four damage categories of broken tips and leading edge notches on one or both blades. The fifth propeller remained undamaged. The damages were gradually increased according to the three defined severity classes. Six independent runs at different battery state of charge were performed for each propeller with a defined damage and severity.

For the analysis, the measured time series data from the test bench runs are segmented into time windows of 0.5 seconds, each with a constant duty cycle input. This ensures that only short measurement samples are needed to detect reduced propeller health. Extracting features from these time series segments filters out the effect of random measurement noise. When the duty cycle remains constant, the median values of consecutive segments differ only slightly from one another. The average percentage variation ranges from 0.1% for the voltage sensor to 2.1% for the current sensor. In a subsequent

Table 2. Measured propeller health index for different types of damage.

Type of damage		Undamaged	Grade A	Grade B	Grade C
Broken tip	One blade	100.7%	93.0%	91.6%	78.8%
Broken tip	Both blades	96.8%	88.7%	82.0%	65.0%
Leading edge notches	One blade	102.3%	101.1%	100.4%	96.0%
Leading edge notches	Both blades	100.8%	101.6%	99.2%	96.9%

data cleaning step, segments with measurement errors falling outside the sensors' measuring range or the drive train's operating range are excluded from the analysis. This is the case for only 0.1% of the total number of segments.

Apart from its effect on generated thrust, propeller damage also affects the measurement data from the voltage, current, and rotational speed sensors. Therefore, statistical features of these sensor measurements are useful inputs to the fault classification. For example, large damage that reduces the diameter of the propeller leads to reduced air resistance, so that higher rotational speeds can be reached at the same input duty cycle. For each time window, the median, peak-to-peak, and skewness values of the supply voltage, current, and rotational speed are calculated and used as features. The open-circuit voltage of the battery with no load is measured before each test bench run and serves as an indicator of the state of charge. Typically, higher open-circuit voltages correspond to a high state of charge, while lower voltages correspond to a low state of charge.

Notably, some damages introduce an increased level of vibration, which can lead to higher stress on the mechanical structure of the test bench or the UAV. This is especially true for a broken tip on one of the blades, which leads to a large imbalance in the system. Figure 5 shows a comparison of the power spectral density of the acceleration measurements of an undamaged propeller and a propeller with a grade C broken tip. The undamaged propeller shows peaks at the blade passing frequency, which is the second order in the order spectrum, and its multiples. Due to its imbalance, the propeller with a broken tip has a very prominent peak at the first order, which corresponds to the rotational frequency. Therefore, both time domain and power spectral density features are extracted from the vibration signal. In the time domain, root mean squared value, peak-to-peak value, and kurtosis are used. Additionally, the power spectral density at the first four multiples of the rotational speed is calculated.

Using the extracted feature set, a random forest classifier from the scikit-learn library (Pedregosa et al., 2011) is trained to estimate the fault category of the tested propellers. During splitting of the data in a training and a test set, it was made sure that data from the same run, that means the same damage and battery state of charge, are kept together and do not

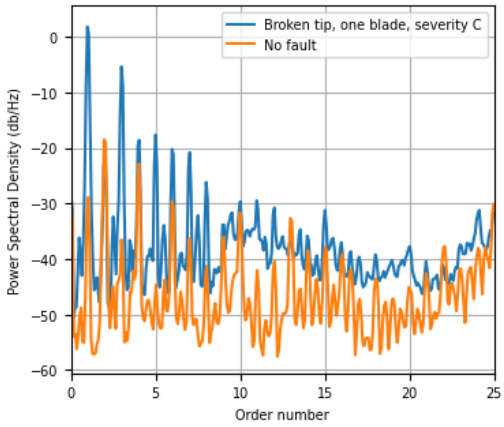

Figure 5. Comparison of power spectral density of an undamaged propeller and a propeller with one broken tip.

appear in both data sets. To reduce the complexity of classification, the task is modeled as a three-class classification problem with the classes being *BrokenTip*, *LeadingEdge* and *NoFault*. Damages to one blade and to both blades are summed up in one class each. For each predicted class, a separate random forest regressor for health estimation is trained using the same input features as for the classification. The health index calculated using the thrust sensor data serves as target value for the health estimation.

5. MODELING RESULTS

This chapter presents the results of the fault classification algorithm and the additional health assessment, beginning with the fault classification.

5.1. Fault Classification

The trained random forest classifier achieves a total accuracy of 91.9% on the hold-out test set. Figure 6 shows the resulting confusion matrix. Undamaged propellers are correctly detected with high confidence, resulting in a recall of 95%. The recall values for the two fault classes are slightly lower at 86% for the propellers with notches at the leading edge and 94% for broken tips. Most misclassifications occur between undamaged propellers and those with leading edge damage. This aligns with the data analysis results from Sec-

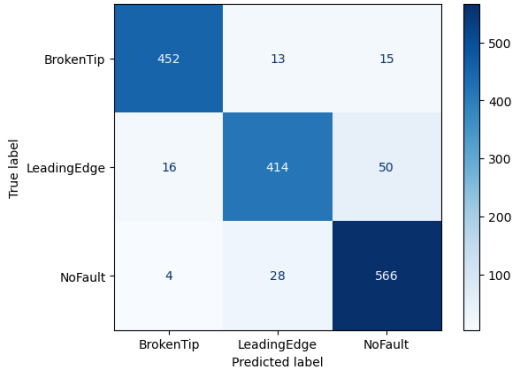

Figure 6. Confusion matrix of the fault classification.

tion 3, which showed that the effects of these damages can be minimal, making them difficult to detect.

Propellers with high imbalance due to a broken tip pose the greatest threat to the safety of UAVs because large vibrations can put high stress on the UAV structure. Of the misclassified measurement samples from propellers with broken tips, only four are due to damage affecting only one blade. This demonstrates that they can be accurately classified using information from vibration signal and power spectral density analysis. When both blades are broken and no imbalance is introduced to the system, the number of misclassified samples increases. However, the vast majority of these samples belong to severity grade A. Damages of severity grade C are always classified correctly. In contrast, misclassifications of leading-edge damage occur at all severity levels and for propellers with one or two damaged blades.

5.2. Health Assessment

Figure 7 depicts the results of the health index estimation. For each propeller with a specific type and severity of damage, the range of predictions from all measurement samples at various battery states of charge is shown. The upper and lower limits of the error bars correspond to the maximum and minimum predicted health indices of all correctly classified measurements. Measurement samples that were misclassified are included as outliers in the graph because they cause the greatest deviation between the predicted and measured health index.

For leading edge notches, where the health index always stays close to 100%, the mean absolute prediction error is 0.61%. This indicates that the remaining health can be estimated with high accuracy. However, misclassifications in the fault classification phase can result in single large errors of up to 25%, as the classification label is one of the most important pieces of information for health index modeling.

The average error for the broken tip propellers is 2.54%. Similar to notch faults, misclassifications from the fault classification stage lead to larger deviations between the predicted and

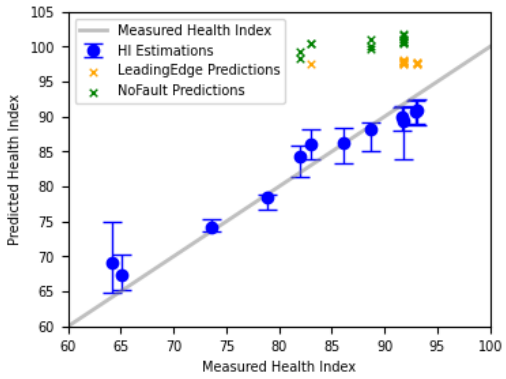

(a) Broken tip damage

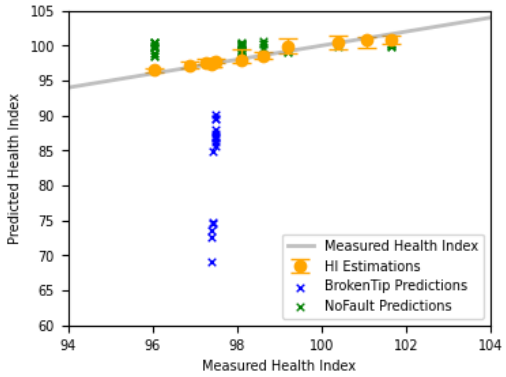

(b) Leading edge notches

Figure 7. Health index prediction for each damaged propeller configuration.

measured health index. Since misclassifications only occur for broken tips of severity grades A and B, this only affects propellers with health indices between 80% and 95%. A high variance in predictions for the same propeller and fault type is especially visible at very high damage. This is due to the limited data in the lower health index ranges. Having more data on severely damaged propellers, as well as more gradations of damage, could help overcome this issue and improve the accuracy of predictions.

In summary, a few high prediction errors are observed for single measurement samples of 0.5 seconds in length. However, the mean error over all measured samples for the same propeller is significantly lower. By including multiple measurement samples and averaging the predicted health indices, outliers in the prediction can be filtered out and the remaining health of the propellers is categorized accurately with low prediction error.

6. CONCLUSION

Minor damage to UAV propellers has a limited impact on the thrust delivered by the drive train. To distinguish between

minor damage and damage that is critical to the operation of UAVs, fault detection algorithms must be complemented by an estimation of fault severity. In this paper, the effect of several types and severity grades of damage is analyzed, and a health index is defined based on these findings. The proposed approach for fault detection and health assessment achieves high accuracy in classifying propeller faults and estimating their remaining health with low prediction error, indicating its potential for further research and application.

In order to improve the developed methods, an extension of the collected dataset is necessary. Increasing the size of the dataset could allow for incorporating and analyzing statistical variations of propellers with the same damage. Moreover, by differentiating between more severity grades, a broader range of possible health index values can be covered in the data, which could improve the results of the health estimation model.

All the data was collected in a test bench environment, which presents several simplifications compared to real UAV applications. Although the test bench is necessary to quantify the effect of damage on delivered thrust and define an appropriate health index, the data does not represent actual UAV flight. During flight, the drive train is controlled in a closed loop. Therefore, the duty cycle input is not held constant as it is in an open-loop test bench environment. Other factors, such as wind or cross-influences from other multicopter drive trains, could also affect the measured vibration data. Future research will focus on extending the developed approach to bring it closer to real flight data. As a first improvement, the approach will be adjusted to work with measurement data that has a non-constant, varying duty cycle.

REFERENCES

Baldini, A., Felicetti, R., Ferracuti, F., Freddi, A., Monteriù, A., Scalella, S., & Zhang, Y. (2024). Multirotor lift estimation under battery discharge and blade faults. In *2024 international conference on unmanned aircraft systems (icuas)* (pp. 8–14). IEEE. doi: 10.1109/ICUAS60882.2024.10556984

Benini, A., Ferracuti, F., Monteriu, A., & Radensleben, S. (2019). Fault detection of a vtol uav using acceleration measurements. In *2019 18th european control conference (ecc)* (pp. 3990–3995). IEEE. doi: 10.23919/ECC.2019.8796198

Bondyra, A., Gasior, P., Gardecki, S., & Kasinski, A. (2017). Fault diagnosis and condition monitoring of uav rotor using signal processing. In *2017 signal processing: Algorithms, architectures, arrangements, and applications (spa)* (pp. 233–238). IEEE. doi: 10.23919/SPA.2017.8166870

Brulin, P.-Y., Khenfri, F., & Rizoug, N. (2024). Generating fault databases through simulated and experimental multi-rotor uav propulsion systems. *IEEE Transactions on Vehicular Technology*, *73*(4), 4671–4682. doi: 10.1109/TVT.2024.3352172

Osborne, M., Lantair, J., Shafiq, Z., Zhao, X., Robu, V., Flynn, D., & Perry, J. (2019). Uas operators safety and reliability survey: Emerging technologies towards the certification of autonomous uas. In *2019 4th international conference on system reliability and safety (icsrs)* (pp. 203–212). IEEE. doi: 10.1109/ICSRS48664.2019.8987692

Pedregosa, F., Varoquaux, G., Gramfort, A., Michel, V., Thirion, B., Grisel, O., ... Édouard Duchesnay (2011). Scikit-learn: Machine learning in python. *Journal of Machine Learning Research*, *12*(85), 2825-2830. Retrieved from `http://jmlr.org/papers/v12/pedregosa11a.html`

Pose, C., Giribet, J., Torre, G., & Marzik, G. (2023). Neural network-based propeller damage detection for multirotors. In *2023 international conference on unmanned aircraft systems (icuas)* (pp. 17–23). IEEE. doi: 10.1109/ICUAS57906.2023.10156355

Pourpanah, F., Zhang, B., Ma, R., & Hao, Q. (2018). Anomaly detection and condition monitoring of uav motors and propellers. In *2018 ieee sensors* (pp. 1–4). IEEE. doi: 10.1109/ICSENS.2018.8589572

Puchalski, R., & Giernacki, W. (2022). Uav fault detection methods, state-of-the-art. *Drones*, *6*(11), 330. doi: 10.3390/drones6110330

Wolfram, D., & Vogel, F. (2017). *Zustandsüberwachung des antriebsstrangs kleiner multikopter zur missionsabhängigen verfügbarkeitsbestimmung* (No. 450077). Retrieved from `https://www.dglr.de/publikationen/2017/450077.pdf`

Wolfram, D., Vogel, F., & Stauder, D. (2018). Condition monitoring for flight performance estimation of small multirotor unmanned aerial vehicles. In *2018 ieee aerospace conference* (pp. 1–17). IEEE. doi: 10.1109/AERO.2018.8396471